

Artificial synapse based on Co_3O_4 nanosheets for high-accuracy pattern recognition

Ying Li(李颖), Xiaofan Zhou(周晓凡), Jiajun Guo(郭家俊), Tong Chen(陈通), Xiaohui Zhang(张晓辉), Xia Xiao(肖夏), Guangyu Wang(王光宇), Mehran Khan Alam, Qi Zhang(张琪), and Liqian Wu(武力乾)

Citation: Chin. Phys. B, 2025, 34 (**12**): 128101. DOI: 10.1088/1674-1056/ae1817
http://cpb.iphy.ac.cn; http://iopscience.iop.org/cpb

What follows is a list of articles you may be interested in

Performance analysis of porous solar absorbers with high-temperature radiation cooling function

Haiyan Yu(于海燕), Anqi Chen(陈安琪), Mingdong Li(李明东), Ahali Hailati(阿哈里·海拉提), Xiaohu Wu(吴小虎), and Xiaohan Ren(任霄汉)
Chin. Phys. B, 2025, 34 (**6**): 068102. DOI: 10.1088/1674-1056/add4e3

Surface-pitted TiN nanoparticles for direct absorption solar collectors

Heng Zhang(张衡), Yuchun Cao(曹玉春), Xiaowen Chen(陈晓文), Qihang Yang(杨起航), Ning Chen(陈宁), and Xiaohu Wu(吴小虎)
Chin. Phys. B, 2025, 34 (**6**): 068101. DOI: 10.1088/1674-1056/ada887

W-doped In_2O_3 nanofiber optoelectronic neuromorphic transistors with synergistic synaptic plasticity

Yang Yang(杨洋), Chuanyu Fu(傅传玉), Shuo Ke(柯硕), Hangyuan Cui(崔航源), Xiao Fang(方晓), Changjin Wan(万昌锦), and Qing Wan(万青)
Chin. Phys. B, 2023, 32 (**11**): 118101. DOI: 10.1088/1674-1056/acdeda

Synaptic plasticity and classical conditioning mimicked in single indium-tungsten-oxide based neuromorphic transistor

Rui Liu(刘锐), Yongli He(何勇礼), Shanshan Jiang(姜珊珊), Li Zhu(朱力), Chunsheng Chen(陈春生), Ying Zhu(祝影), and Qing Wan(万青)
Chin. Phys. B, 2021, 30 (**5**): 058102. DOI: 10.1088/1674-1056/abc163

A synaptic transistor with $NdNiO_3$

Xiang Wang(汪翔), Chen Ge(葛琛), Ge Li(李格), Er-Jia Guo(郭尔佳), Meng He(何萌), Can Wang(王灿), Guo-Zhen Yang(杨国桢), Kui-Juan Jin(金奎娟)
Chin. Phys. B, 2020, 29 (**9**): 098101. DOI: 10.1088/1674-1056/aba60c

---

Artificial synapse based on Co_3O_4 nanosheets for high-accuracy pattern recognition

Ying Li(李颖)[1], Xiaofan Zhou(周晓凡)[1], Jiajun Guo(郭家俊)[1,†], Tong Chen(陈通)[2,3], Xiaohui Zhang(张晓辉)[1], Xia Xiao(肖夏)[1], Guangyu Wang(王光宇)[1,‡], Mehran Khan Alam[4], Qi Zhang(张琪)[5], and Liqian Wu(武力乾)[6,§]

[1] *School of Physical Science and Information Technology, Liaocheng University, Liaocheng* 252059, *China*
[2] *School of Materials Science and Engineering, Zhejiang University, Hangzhou* 310027, *China*
[3] *Institute of Advanced Semiconductors, Hangzhou Innovation Center, Zhejiang University, Hangzhou* 311200, *China*
[4] *Key Laboratory for Liquid-Solid Structural Evolution and Processing of Materials (Ministry of Education), School of Materials Science and Engineering, Shandong University, Jinan* 250061, *China*
[5] *School of Medical Information Engineering, Department of Physics, Jining Medical University, Jining* 272067, *China*
[6] *Wenzhou Institute of Hangzhou Dianzi University, Wenzhou* 325038, *China*

(Received 22 July 2025; revised manuscript received 22 September 2025; accepted manuscript online 28 October 2025)

Two-dimensional (2D) metal oxides are promising candidates for constructing neuromorphic systems because of their intriguing physical properties, such as atomic thinness and ionic activity. In this work, Co_3O_4 nanosheets were synthesized using a solvothermal method and integrated into artificial synapses. Based on the synaptic plasticity of the Co_3O_4 nanosheet-based memristive device, an artificial neural network (ANN) was designed and tested. A recognition accuracy of approximately 96% was achieved for the Modified National Institute of Standards and Technology (MNIST) handwritten digit classification task using this ANN. These results highlight the potential of Co_3O_4 nanosheet-based artificial synapses and Al/Co_3O_4 nanosheet/ITO memristor devices as excellent material candidates for neuromorphic hardware.

Keywords: artificial synapse, memristor, Co_3O_4 nanosheet, synaptic plasticity

PACS: 81.07.−b, 84.35.+i, 85.35.−p, 73.40.Rw

DOI: 10.1088/1674-1056/ae1817 **CSTR:** 32038.14.CPB.ae1817

1. Introduction

Neuromorphic computing, drawing inspiration from the information-processing capabilities of the brain, holds promise to surpass the von Neumann model in managing complex tasks via massive parallelism with low energy consumption.[1–7] Crucial components like artificial synapses play a vital role in hardware-based neuromorphic computing, enabling the emulation of connection strength changes between processing neurons.[8,9] The memristor, functioning as an electronic artificial synapse with a structure resembling that of biological synapses, can modulate conductance in response to electrical stimuli, effectively mimicking synaptic plasticity and neuronal sensing functions.[10–12] Various materials, including binary metal oxides,[13–15] polymers,[16,17] molecules,[18–20] and perovskites,[21–23] have been proposed for memristor fabrication. Recently, the use of two-dimensional (2D) materials in memristor construction has garnered significant research interest due to their diverse elemental composition, facile processability, and tunable physicochemical properties.[24–27]

Co_3O_4 nanosheets, a type of 2D material, have been widely utilized in various applications, including batteries, supercapacitors, and heterogeneous catalysis.[28–30] In particular, using Co_3O_4 nanosheets as a dielectric medium in memristors has demonstrated excellent resistive switching effects.[31] Moreover, Co_3O_4 nanosheets, as binary metal oxides, possess inherent advantages for integration with complementary metal–oxide–semiconductor (CMOS) technology.[32] The redox-active nature of Co_3O_4 nanosheets makes them exceptional solid electrolytes for ion transport, exhibiting behavior akin to neurotransmitters in biological synapses.[6,32] Despite the merits of Co_3O_4 nanosheets as 2D materials and metal oxides, research on their application in neuromorphic devices remains limited. Therefore, exploring the potential of Co_3O_4 nanosheets in artificial synapses and their applications in neuromorphic computing is imperative.

In this work, the Co_3O_4 nanosheet-based memristive device, constructed in a sandwich structure with Al/Co_3O_4 nanosheet/ITO electrodes, was used to simulate the behavior of artificial synapses. The electric-field-driven migration of oxygen ions in Co_3O_4 nanosheets dynamically controls the current passing through the junction. To explore the potential of the Co_3O_4 nanosheet-based artificial synapses for pattern recognition tasks, an artificial neural network (ANN) was de-

†Corresponding author. E-mail: guojiajun@lcu.edu.cn
‡Corresponding author. E-mail: wangguangyu@lcu.edu.cn
§Corresponding author. E-mail: wulq@hdu.edu.cn

© 2025 Chinese Physical Society and IOP Publishing Ltd. All rights, including for text and data mining, AI training, and similar technologies, are reserved.

signed and tested. Benefiting from the long-term potentiation and depression characteristics of the Co_3O_4 nanosheet-based device, the ANN demonstrated the ability to perform complex tasks, achieving approximately 96% recognition accuracy for the Modified National Institute of Standards and Technology (MNIST) handwritten digit classification task. These results highlight Co_3O_4 nanosheet-based artificial synapses and Al/Co_3O_4 nanosheet/ITO memristor devices as excellent material candidates for neuromorphic hardware.

2. Method

The Co_3O_4 nanosheets were synthesized via a solvothermal method. Briefly, $Co(NO_3)_2{\cdot}6H_2O$ (5 mmol) and urea (20 mmol) were dissolved in deionized water (15 mL) and ethylene glycol (105 mL). The mixture was stirred at 80 °C for 12 h. The resulting precipitate was collected and washed several times with distilled water and ethanol. The precursor was then dried in a vacuum oven at 60 °C for 12 h. Co_3O_4 nanosheets were obtained by calcination in air at 300 °C for 2 h.

Before electrode assembly, a glass substrate coated with an ITO electrode (thickness: 180 nm) was sequentially cleaned with ethanol and deionized water. Large-area 2D van der Waals thin films based on Co_3O_4 nanosheets were then fabricated via a spin-coating technique.[33,34] Briefly, the aqueous Co_3O_4 nanosheet solution was spin-coated onto the ITO substrate at 500 rpm for 5 s and 1000 rpm for 60 s, followed by annealing on a hot plate at 100 °C for 30 min. To fabricate the Al/Co_3O_4 nanosheet/ITO device, Al electrodes (thickness: 80 nm) were deposited onto the Co_3O_4 nanosheet thin film via thermal evaporation using a dot-patterned shadow mask (diameter: 200 μm).

The morphology and structure of the samples were characterized using transmission electron microscopy (TEM) and high-resolution transmission electron microscopy (HRTEM) with a field-emission transmission electron microscope (FE-TEM, JEOL JEM-2100F), along with energy-dispersive x-ray spectroscopy (EDS) for signal detection and mapping. Raman spectra were recorded using a Thermo Fisher high-resolution confocal Raman microscope. Ultraviolet–visible (UV–vis) absorption spectra were obtained using a spectrophotometer (U-3310, Hitachi). Electrical measurements of the Al/Co_3O_4 nanosheet/ITO devices were performed using a semiconductor parameter analyzer (Agilent B1500A) and a Keithley 2400 source meter.

3. Results and discussion

Figure 1(a) presents the TEM image and HRTEM micrograph of the Co_3O_4 nanosheets. The TEM image reveals a clear network-like morphology of the Co_3O_4 nanosheets, while the HRTEM image displays distinct lattice fringes with a spacing of 0.28 nm, corresponding to the (220) crystallographic planes of Co_3O_4, indicating a high-quality crystalline structure.

For the EDS measurements, the Co_3O_4 nanosheet suspension was deposited onto a porous carbon-coated copper grid in a cleanroom environment to prevent contamination, and a 200-keV electron beam was used to minimize radiation damage. The EDS spectrum corresponding to the elemental mapping image of the Co_3O_4 nanosheet is shown in Fig. 1(b). The prominent background peaks can be attributed to the C and Cu elements from the copper grid, while other minor background peaks can be ignored. Thus, the homogeneous distribution of Co and O elements is confirmed.

Figure 1(c) shows the Raman spectrum of the Co_3O_4 nanosheets. Five characteristic peaks at 190 cm^{-1}, 467 cm^{-1}, 510 cm^{-1}, 608 cm^{-1}, and 672 cm^{-1} are assigned to the F_{2g}, E_g, F_{2g}, F_{2g}, and A_{1g} vibrational modes of the spinel Co_3O_4 structure, respectively.[35,36]

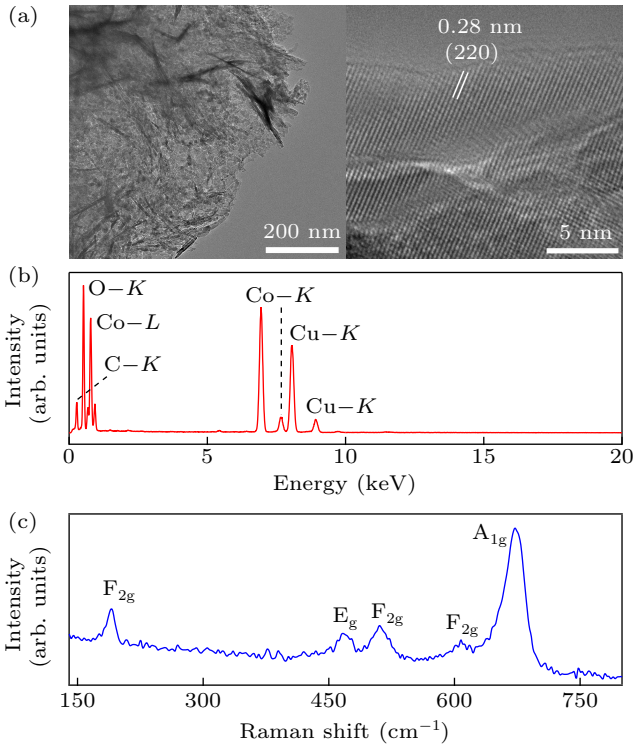


Fig. 1. (a) TEM image (left) and HRTEM micrograph (right) of the Co_3O_4 nanosheets. (b) EDS spectrum of the Co_3O_4 nanosheets. (c) Raman spectra of the Co_3O_4 nanosheets.

Next, the optical properties of the Co_3O_4 nanosheets were characterized using UV–vis spectroscopy. As shown in Fig. 2, the absorbance spectrum of the Co_3O_4 nanosheets reveals two distinct optical absorption bands centered around 270 nm and 400 nm, consistent with previous reports for Co_3O_4 nanosheets.[37–39] These absorption bands are attributed to ligand-to-metal charge transfer transitions in Co_3O_4. The inset of Fig. 2 shows a Tauc plot of the UV–vis absorption spectrum. Based on the Kubelka–Munk equation,[40,41] the optical

band gaps (E_g) of the Co_3O_4 nanosheets are determined to be 2.0 eV and 3.56 eV, respectively. The first band corresponds to the $O^{2-} \rightarrow Co^{2+}$ charge-transfer process, which represents the fundamental valence-to-conduction band excitation,[42,43] whereas the second band corresponds to the $O^{2-} \rightarrow Co^{3+}$ charge-transfer transition, as the Co^{3+} level lies below the conduction band.[44,45]

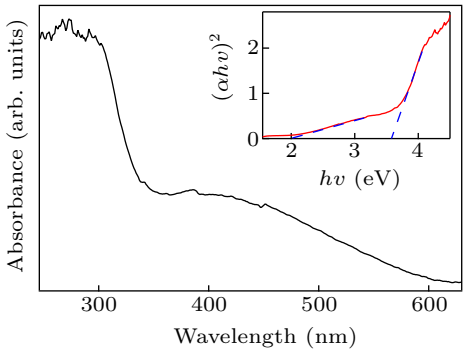


Fig. 2. UV–vis absorption spectrum and the corresponding $(\alpha hv)^2$–hv Tauc plot (inset) of the Co_3O_4 nanosheets.

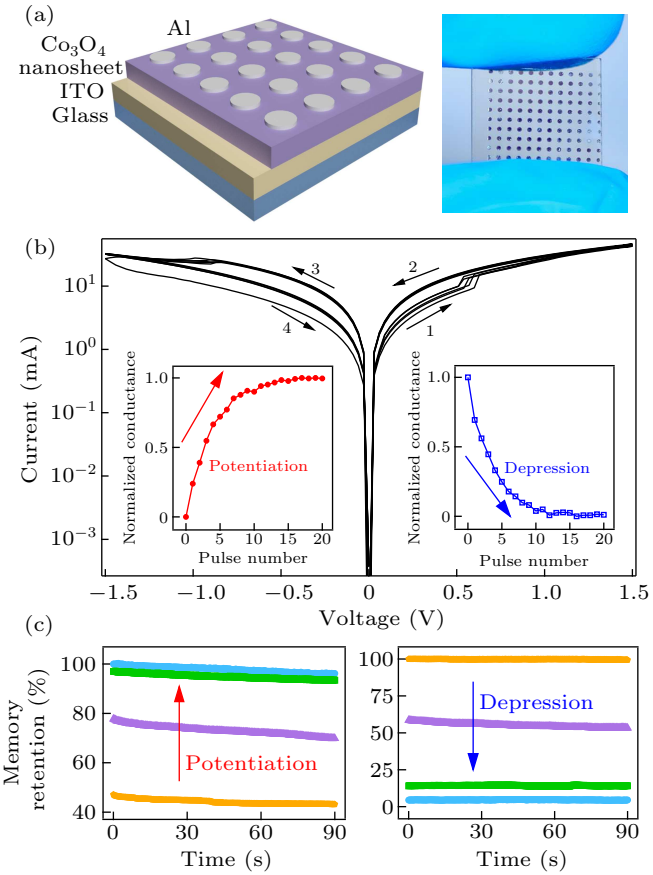


Fig. 3. (a) The schematic diagram and photograph of Al/Co_3O_4 nanosheet/ITO device. (b) Consecutive *I*–*V* characteristics of the Al/Co_3O_4 nanosheet/ITO device, along with the potentiation and depression behavior of the Al/Co_3O_4 nanosheet/ITO device under 0.6 V and −0.6 V pulses of 300 µs, respectively (inset). (c) The memory retention properties of the Al/Co_3O_4 nanosheet/ITO device, corresponding to the potentiation (left) and depression (right) behaviors, after potentiated and depressed by 3 pulses, 6 pulses, 15 pulses, and 20 pulses.

Figure 3(a) shows the schematic diagram and photograph of the Al/Co_3O_4 nanosheet/ITO device, which exhibits a typical sandwich structure, with the top Al electrode and bottom ITO electrode sandwiching the Co_3O_4 nanosheet layer. Figure 3(b) shows the typical current–voltage (*I*–*V*) characteristics of the Al/Co_3O_4 nanosheet/ITO device, measured with five voltage sweeps from 0 V to 1.5 V, then to −1.5 V, and back to 0 V. The device exhibits clear bipolar switching behavior, occurring without the need for an electroforming process, as evidenced by the pronounced hysteresis loop, demonstrating its capability to switch between distinct conductive states — an essential feature for memory and switching applications.

In biological neural systems, a synapse is a junction that connects the presynaptic and postsynaptic neurons, enabling signal transmission through neurotransmitter release. Analogously, the two electrodes in the Al/Co_3O_4 nanosheet/ITO device can be considered as the presynaptic and postsynaptic terminals. As shown in the inset of Fig. 3(b), the device conductance progressively increases and decreases upon the application of 20 consecutive voltage pulses (width: 300 µs; amplitude: 0.6 V and −0.6 V). This pulsed operation induces reversible conductance modulation, closely mimicking the synaptic plasticity observed in biological systems. In addition, the memory retention properties of the Al/Co_3O_4 nanosheet/ITO device corresponding to the potentiation (left) and depression (right) behaviors, after potentiated and depressed by 3 pulses, 6 pulses, 15 pulses, and 20 pulses, are shown in Fig. 3(c). As the number of pulses increases, the synaptic weight is retained for a longer duration with slower decay.

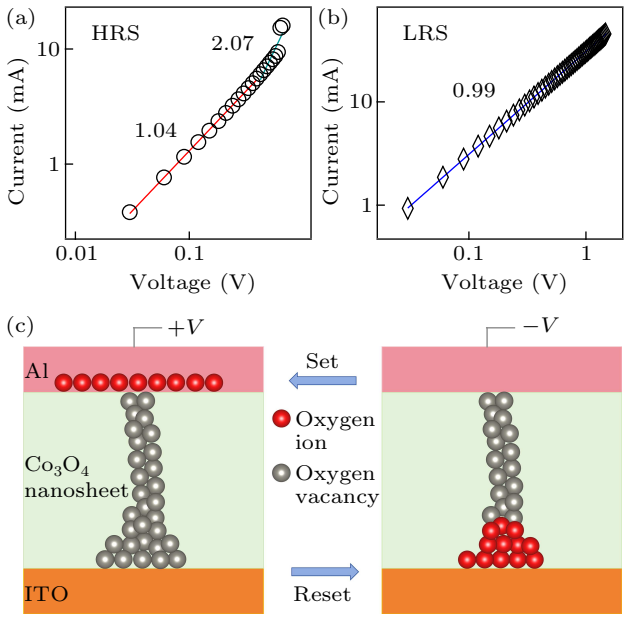


Fig. 4. Fitted *I*–*V* curves of the Al/Co_3O_4 nanosheet/ITO device at the HRS (a) and LRS (b). (c) Schematic illustration of the formation and rupture of oxygen-vacancy conductive filaments in the Al/Co_3O_4 nanosheet/ITO device.

Such behavior is reminiscent of long-term potentiation (LTP) and long-term depression (LTD) in biological synapses,

where synaptic strength is strengthened or weakened depending on the stimulation frequency and pattern. Therefore, the Al/Co_3O_4 nanosheet/ITO device shows potential as a memristive synaptic element for neuromorphic computing applications.

Moreover, as shown in Fig. 4(a), the fitted *I*–*V* curve clearly exhibits two distinct high resistance state (HRS) regions: an ohmic region at low voltages, followed by a quadratic region up to the set voltage. This behavior indicates that the conduction mechanism is trap-controlled space-charge-limited conduction (SCLC).[46] In contrast, the fitted result in the low resistance state (LRS) reveals ohmic conduction behavior throughout the entire voltage-sweeping range (Fig. 4(b)).

In recent years, oxide-based resistive switching behaviors have been reported to originate from two types of mechanisms: (1) filamentary resistive switching, in which oxygen vacancies form conductive filaments bridging the two electrodes, and (2) interface-type switching, in which oxygen vacancies are distributed along an interface, modulating the device conductivity.[47,48] The resistive switching behavior observed in the Al/Co_3O_4 nanosheet/ITO device is attributed to the filamentary mechanism, as supported by the following observations: (1) as shown in Fig. 3(b), the bipolar *I*–*V* curve exhibits an abrupt current jump at the set and reset transitions, a hallmark of filamentary resistive switching,[49–52] in contrast to the smooth *I*–*V* variation typical of interface-type switching;[49–51] and (2) the LRS of the Al/Co_3O_4 nanosheet/ITO device displays ohmic behavior with a slope close to unity (Fig. 4(b)), consistent with filamentary conduction characteristics.[53–55]

The schematic illustration of the switching mechanism based on oxygen-vacancy conductive filaments in the Al/Co_3O_4 nanosheet/ITO device is shown in Fig. 4(c). When a positive bias is applied to the Al electrode, negatively charged oxygen ions are extracted from the Co_3O_4 nanosheet layer and migrate toward the Al electrode, generating additional oxygen vacancies. These newly formed and preexisting oxygen vacancies promote the formation of conductive filaments, switching the device to the LRS. Moreover, Al, as a chemically active electrode that can react with oxygen ions, consumes oxygen from the oxide layer, promoting the formation of oxygen vacancies,[56] which contributes to the development of vacancy conductive filaments.[57] Conversely, when a negative bias is applied to the Al electrode, oxygen ions migrate back into the Co_3O_4 nanosheet layer, recombining with the oxygen-deficient filaments and rupturing the conductive paths, thereby resetting the device to the HRS.

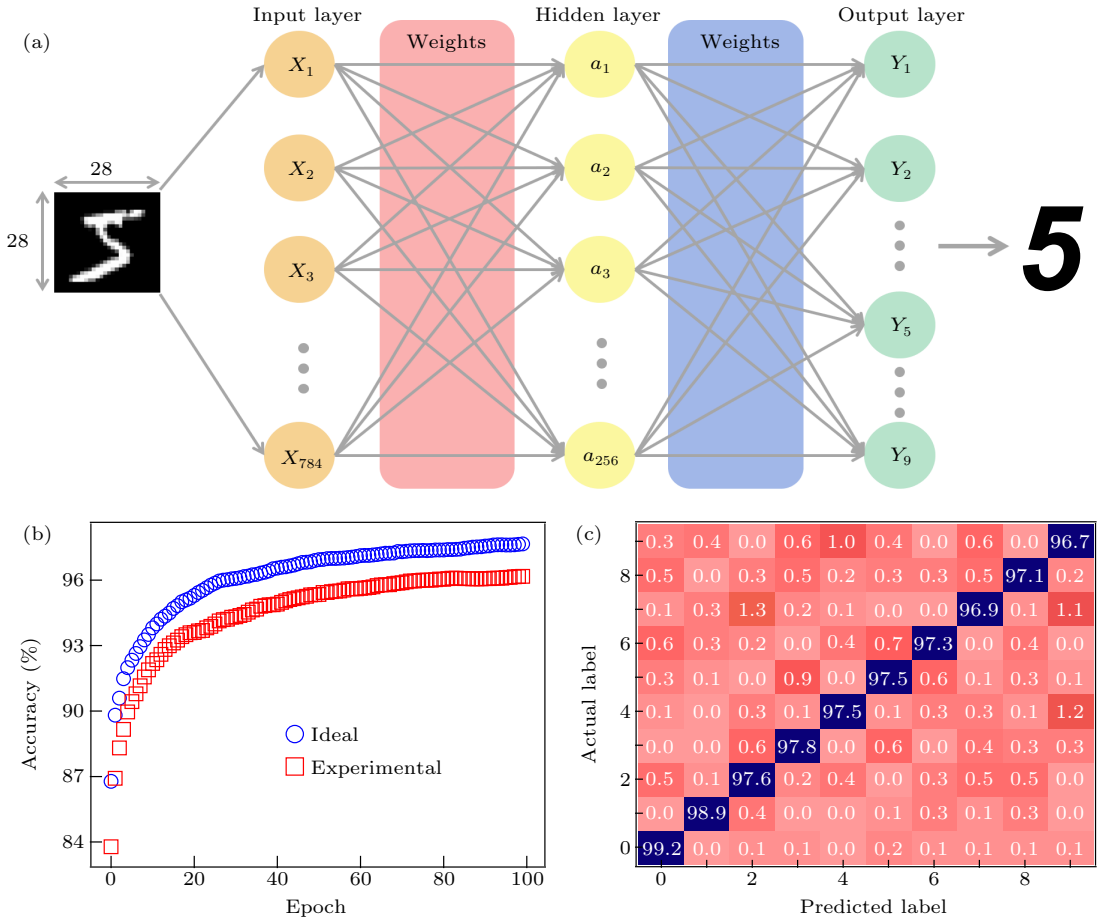


Fig. 5. (a) Schematic diagram of the ANN architecture used for MNIST digit classification. (b) Training accuracy as a function of the number of epochs. (c) Confusion matrix showing the recognition accuracy of the handwritten digits.

The synaptic behavior of the Al/Co_3O_4 nanosheet/ITO device can also be explained by this oxygen-vacancy filamentary mechanism. The device conductance can be modulated — either increased (analogous to LTP) or decreased (analogous to LTD) — through the formation, rupture, or size modulation of conductive filaments induced by oxygen-ion migration under electrical stimulation.

To evaluate the computing capability of the proposed Al/Co_3O_4 nanosheet/ITO memristive device, the MNIST handwritten digit dataset was employed to design and assess an ANN for pattern recognition.[58] Figure 5(a) shows the schematic diagram of the ANN architecture, which consists of an input layer with 784 neurons (each representing one pixel in the 28×28 input image), a hidden layer with 256 neurons, and an output layer with 10 neurons corresponding to digits 0–9. The model was trained on 60000 images from the MNIST training dataset to optimize the synaptic weights and accurately classify handwritten digits, and its performance was evaluated using 10000 images from the testing dataset.

Figure 5(b) presents the recognition accuracy curves of the ANN for handwritten digits. The ideal accuracy steadily increases with training and reaches approximately 98% after 100 epochs. Although the experimental accuracy is slightly lower than the ideal value, it stabilizes around 96%, demonstrating the excellent potential of the Al/Co_3O_4 nanosheet/ITO device for ANN-based handwritten digit recognition.

Figure 5(c) shows the confusion matrix of the handwritten digit recognition model based on the modified MNIST dataset, where the ANN based on the Al/Co_3O_4 nanosheet/ITO device achieves high accuracy in recognizing each digit, ranging from 96.7% to 99.2%.

4. Conclusion

In summary, Co_3O_4 nanosheets were successfully synthesized via a solvothermal method and used to fabricate a memristor for artificial synaptic functions in neuromorphic systems. The device exhibited pronounced synaptic plasticity, effectively mimicking the behavior of biological synapses. Furthermore, an ANN was designed and trained using the MNIST dataset. The results showed that the ANN, benefiting from the unique properties of the Co_3O_4 nanosheet-based artificial synapses, achieved a recognition accuracy of approximately 96% for handwritten digit classification, demonstrating the strong potential of these devices in complex pattern recognition tasks. These findings highlight Co_3O_4 nanosheet-based artificial synapses and Al/Co_3O_4 nanosheet/ITO memristor devices as excellent candidates for energy-efficient neuromorphic hardware with broad applications in artificial intelligence and cognitive computing.

Acknowledgments

This work was supported by the Natural Science Foundation of Shandong Province (Grant Nos. ZR2024MA019 and ZR2023QA106) and the "Pioneer" and "Leading Goose" R&D Program of Zhejiang (Grant No. 2023C01018).

References

[1] Merolla P A, Arthur J V, Alvarez-Icaza R, *et al.* 2014 *Science* **345** 668
[2] Ielmini D and Wong H S P 2018 *Nat. Electron.* **1** 333
[3] Sebastian A, Gallo M L, Khaddam-Aljameh R and Eleftheriou E 2020 *Nat. Nanotechnol.* **15** 529
[4] Liu K, Zhang T, Dang B, Bao L, Xu L, Cheng C, Yang Z, Huang R and Yang Y 2022 *Nat. Electron.* **5** 761
[5] Wang P, Chen M, Xie Y, Pan C, Watanabe K, Taniguchi T, Cheng B, Liang S J and Miao F 2023 *Chin. Phys. Lett.* **40** 117201
[6] Yu Y T and Yang X L 2023 *Chin. Phys. B* **32** 030201
[7] Yang Y, Zhao J, Liu Y, Hua X, Wang T, Zheng J, Hao Z, Xiong B, Sun C and Han Y 2024 *Chin. Phys. B* **33** 030702
[8] Roy K, Jaiswal A and Panda P 2019 *Nature* **575** 607
[9] Zhu J, Zhang T, Yang Y and Huang R 2020 *Appl. Phys. Rev.* **7** 011312
[10] Xia Q and Yang J J 2019 *Nat. Mater.* **18** 309
[11] Zhou Z, Zhao J, Chen A P, Pei Y, Xiao Z, Wang G, Chen J and Yan X 2020 *Mater. Horiz.* **7** 1106
[12] Li J, Qian Y, Li W, Yu S, Ke Y, Qian H, Lin Y, Hou C, Shyue J, Zhou J, Chen Y, Xu J, Zhu J, Yi M and Huang W 2023 *Adv. Mater.* **35** 2209728
[13] Tan Z H, Yang R, Terabe K, Yin X B, Zhang X D and Guo X 2016 *Adv. Mater.* **28** 377
[14] Ryu J H and Kim S 2020 *Chaos Solitons Fractals* **140** 110236
[15] Wang J, Teng C, Zhang Z, Chen W, Tan J, Pan Y, Zhang R, Zhou H, Ding B, Cheng H and Liu B 2021 *ACS Nano* **15** 15123
[16] Keene S T, Lubrano C, Kazemzadeh S, Melianas A, Tuchman Y, Polino G, Scognamiglio P, Lucio C, Alberto S, van de Burgt Y and Santoro F 2020 *Nat. Mater.* **19** 969
[17] Zhang B, Chen W, Zeng J, Fan F, Gu J, Chen X, Yan L, Xie G, Liu S, Yan Q, Baik S J, Zhang Z G, Chen W, Hou J, El-Khouly M E, Zhang Z, Liu G and Chen Y 2021 *Nat. Commun.* **12** 1984
[18] Zhang K, Wang C, Zhang M, *et al.* 2020 *Nat. Nanotechnol.* **15** 1019
[19] Han Y, Nickle C, Zhang Z, Astier H P A G, Duffin T J, Qi D, Wang Z, del Barco E, Thompson D and Nijhuis C A 2020 *Nat. Mater.* **19** 843
[20] Zhang Y, Liu L, Tu B, Cui B, Guo J, Zhao X, Wang J and Yan Y 2023 *Nat. Commun.* **14** 247
[21] Xiao Z, Yuan Y, Shao Y, Wang Q, Dong Q, Bi C, Sharma P, Gruverman A and Huang J 2015 *Nat. Mater.* **14** 193
[22] Zhao X, Xu H, Wang Z, Lin Y and Liu Y 2019 *InfoMat* **1** 183
[23] Mao J Y, Zheng Z, Xiong Z Y, Huang P, Ding G L, Wang R, Wang Z P, Yang J Q, Zhou Y, Zhai T and Han S T 2020 *Nano Energy* **71** 104616
[24] Shi Y, Liang X, Yuan B, Chen V, Li H, Hui F, Yu Z, Yuan F, Pop E, Wong H S P and Lanza M 2018 *Nat. Electron.* **1** 458
[25] Huh W, Lee D and Lee C H 2020 *Adv. Mater.* **32** 2002092
[26] Peng Z, Cheng Z, Ke S, Xiao Y, Ye Z, Wang Z, Shi T, Ye C, Wen X, Chu P K, Yu X F and Wang J 2023 *Adv. Funct. Mater.* **33** 2211269
[27] Zhong J, Lin X, Sun H, Wang F, Liu K, Wei J, Li Z, Ji Y, Liu P, Liu W and Zhang K 2024 *Appl. Surf. Sci.* **678** 161050
[28] Zou Y, Kinloch I A and Dryfe R A W 2015 *ACS Appl. Mater. Interfaces* **7** 22831
[29] Li J, Li Z, Ning F, Zhou L, Zhang R, Shao M and Wei M 2018 *ACS Omega* **3** 1675
[30] Wang X, Li R, Luo X, Mu J, Peng J, Yan G, Wei P, Tian Z, Huang Z and Cao Z 2024 *J. Colloid Interface Sci.* **654** 454
[31] Younis A, Chu D, Lin X, Lee J and Li S 2013 *Nanoscale Res. Lett.* **8** 36
[32] Zhou K, Shang G, Hsu H H, Han S T, Roy V A L and Zhou Y 2023 *Adv. Mater.* **35** 2207774
[33] Tan C, Liu Z, Huang W and Zhang H 2015 *Chem. Soc. Rev.* **44** 2615
[34] Liao L, Kovalska E, Regner J, Song Q and Sofer Z 2024 *Small* **20** 2303638
[35] Wang J, Gao R, Zhou D, Chen Z, Wu Z, Schumacher G, Hu Z and Liu X 2017 *ACS Catal.* **7** 6533
[36] Chen X, Zhong C, Liu B, Liu Z, Bi X, Zhao N, Han X, Deng Y, Lu J and Hu W 2018 *Small* **14** 1702987

[37] Kaviyarasu K, Raja A and Devarajan P A 2013 *Spectrochim. Acta A Mol. Biomol. Spectrosc.* **114** 586
[38] Mao Y, Li W, Liu P, Chen J and Liang E 2014 *Mater. Lett.* **134** 276
[39] Wu B, Shan C, Zhang X, Zhao H, Ma S, Shi Y, Yang J, Bai H and Liu Q 2021 *Appl. Surf. Sci.* **543** 148677
[40] Kubelka P and Munk F 1931 *Tech. Phys.* **12** 593
[41] Dare-Edwards M P, Goodenough J B, Hamnett A and Trevellick P R 1983 *J. Chem. Soc. Faraday Trans.* **79** 2027
[42] Barreca D, Massignan C, Daolio S, Fabrizio M, Piccirillo C, Armelao L and Tondello E 2001 *Chem. Mater.* **13** 588
[43] Gu F, Li C, Hu Y and Zhang L 2007 *J. Cryst. Growth* **304** 369
[44] He T, Chen D, Jiao X, Wang Y and Duan Y 2005 *Chem. Mater.* **17** 4023
[45] Farhadi S, Safabakhsh J and Zaringhadam P 2013 *J. Nanostruct. Chem.* **3** 1
[46] Shang D S, Wang Q, Chen L D, Dong R, Li X M and Zhang W Q 2006 *Phys. Rev. B* **73** 245427
[47] Waser R, Dittmann R, Staikov G and Szot K 2009 *Adv. Mater.* **21** 2632
[48] Kim S, Han J, Kim H, Kim S and Jang H 2018 *Adv. Mater. Technol.* **3** 1800457
[49] Sassine G, Barbera S, Najjari N, Minvielle M, Dubourdieu C and Alibart F 2016 *J. Vac. Sci. Technol. B* **34** 012202
[50] Guo J, Ren S, Wu L, Kang X, Chen W and Zhao X 2018 *Appl. Surf. Sci.* **434** 1074
[51] Han J, Le Q, Choi J, Kim H, Kim S, Hong K, Moon C, Kim T, Kim S and Jang H 2019 *ACS Appl. Mater. Interfaces* **11** 8155
[52] Song L W, Niu S S, Sun Y C, Hua L F, Zhao X and Chen W 2014 *Appl. Phys. Lett.* **104** 093502
[53] Choi J S, Kim J S, Hwang I R, Hong S H, Jeon S H, Kang S O, Park B H, Kim D C, Lee M J and Seo S 2009 *Appl. Phys. Lett.* **95** 022109
[54] Yang Y C, Pan F, Liu Q, Liu M and Zeng F 2009 *Nano Lett.* **9** 1636
[55] Peng H Y, Li G P, Ye J Y, Wei Z P, Zhang Z, Wang D D, Xing G Z and Wu T 2010 *Appl. Phys. Lett.* **96** 192113
[56] Zhou C W, Wu C C, Hsu T H and Huang C L 2025 *Mater. Sci. Semicond. Process.* **185** 108937
[57] Nakamura H and Asai Y 2016 *Phys. Chem. Chem. Phys.* **18** 8820
[58] Ismail M, Rasheed M, Park Y, Lee S, Mahata C, Shim W and Kim S 2024 *J. Chem. Phys.* **161** 134702